The Astrophysical Journal, 891:50 (13pp), 2020 March 1 https://doi.org/10.3847/1538-4357/ab70b1

The 3D Distribution of Long-period Mira Variables in the Galactic Disk*

Riku Urago[1], Toshihiro Omodaka[1], Takahiro Nagayama[1], YuKi Watabe[1], Ryo Miyanosita[1], Noriyuki Matsunaga[2], and Ross A. Burns[3,4]
[1] Department of Physics and Astronomy, Graduate school of Science and Engineering, Kagoshima University, 1-21-35 Korimoto, Kagoshima 890-0065, Japan
k4841512@kadai.jp
[2] Department of Astronomy, The University of Tokyo, 7-3-1 Hongo, Bunkyo-ku, Tokyo 113-0033, Japan
[3] Mizusawa VLBI Observatory, National Astronomical Observatory of Japan, 2-21-1 Osawa, Mitaka, Tokyo 181-8588, Japan
[4] Korea Astronomy and Space Science Institute, 776 Daedeokdae-ro, Yuseong-gu, Daejeon 34055, Republic of Korea
Received 2019 April 5; revised 2020 January 16; accepted 2020 January 17; published 2020 March 3

Abstract

Long-period Mira variable stars are considered to have relatively high initial masses and may be potentially useful as tracers of spiral arm structure of the Milky Way. From 2004 to 2017, we monitored long-period Mira candidates selected from the *IRAS* color–color diagram in the near-infrared K' band. As an initial result of this study, we found 108 Mira variables and determined their periods, mean magnitudes, and amplitudes. Most of them are located between 0° and 90° in Galactic longitude. The peak of their period distribution is at around 500 days, which is longer than the typical value for Mira variables selected in optical surveys. Distances to our Mira variables have also been estimated using the period–luminosity relation (PLR) in 3.4 μm with the help of a three-dimensional map of interstellar extinction. While the K_s-band PLR has a large scatter at longer periods ($\log P > 2.6$), the PLR based on the *Wide-field Infrared Survey Explorer* 3.4 μm data has a much smaller scatter. We compare the spatial distribution of our sample to the spiral arms in the literature, and discuss the possible association of the long-period Mira variables with the spiral arms although the limited spatial coverage and the limited distance accuracy of the current sample prevent us from drawing a firm conclusion.

Unified Astronomy Thesaurus concepts: Milky Way Galaxy (1054); Asymptotic giant branch stars (2100); Distance indicators (394); Spiral arms (1559); Mira variable stars (1066)

1. Introduction

From our perspective within the Galactic disk, it is difficult to establish the large-scale and detailed structure of the Milky Way. Many studies have been done using methods of estimating distances of various tracers of the Galactic structures, for example, H I gas and star-forming regions (SFRs; Kerr 1961). Since the Milky Way is composed of stars and gas, it is necessary to study the distribution of both components to obtain a complete view of Galactic structure. Regarding the stellar component, different tracers should be used for different stellar populations; for example, red clump stars are suitable tracers of old stellar populations in the bulge (e.g., Weiland et al. 1994; Lopez-Corredoira et al. 1997). Mira variables are also good tracers of the bulge, and several previous works investigated their distribution (e.g., Matsunaga et al. 2005; Catchpole et al. 2016). On the other hand, the spiral arms are typically traced by using high-mass SFRs (HMSFR, Burns et al. 2014; Reid et al. 2014, etc.) and classical Cepheids (Gozha & Marsakov 2013; Dambis et al. 2015). In the effort of revealing the spiral arm and the disk structure of the Milky Way, young tracers are important. However, they are also rarer relative to old objects, which tends to prevent us from establishing a detailed map of a young stellar population. In this work, we focus on Mira variables which are abundant throughout the Milky Way; they are more numerous than HMSFRs by a few orders of magnitude (LPV catalog in Milky Way; e.g., Watson et al. 2006; Mowlavi et al. 2018) (HMSFR, Reid et al. 2014).

Mira variables are a class of late-type and long-period variable (LPV) stars that populate the coolest and most luminous part of the asymptotic giant branch (AGB). They have long pulsation periods (Period > 100 days) and large amplitude variations ($\Delta V > 2.5$ mag, $\Delta K > 0.4$ mag). The AGB is the final evolutionary phase of low- to intermediate-mass (1–8 $M_\odot$) stars before the start of the envelope ejection (Habing & Olofsson 2003). The period of Mira variables is a good indicator of its age and initial mass, M_i (Feast & Whitelock 2000; Feast 2008); the shortest period Mira variables (some of which are found in metal-rich globular clusters) are very old with $M_i < 1\ M_\odot$, while the bulk of Mira variables in the solar neighborhood with $\log P \sim 2.5$ are ~7 Gyr old. An age of ~3 Gyr has been estimated to be $\log P \sim 2.65$ and longer period Mira variables (including OH/IR stars which typically are also long-period Mira variables) are even younger (~100 Myr) (Catchpole et al. 2016). Due to their short lifetime, we can reasonably assume that the longer period Mira variables are still located close to the spiral arms where they formed. Furthermore, Mira variables are bright at infrared wavelengths meaning they can be seen through the Galactic disk.

The period–luminosity relation (PLR) of Mira variables has been widely used as a distance indicator since it was established by Glass & Evans (1981) and Feast et al. (1989). As discovered by Wood (2000), AGB variables lie on several parallel sequences in the K band PL diagram, where each sequence corresponds to a particular pulsation mode. Mira variables have larger amplitudes than semi-regular variables and mostly fall on the PL relation corresponding to the fundamental pulsation mode (the sequence C in Wood 2000). However, Mira variables with longer periods ($P > 400$ days) tend to have thick circumstellar dust shells and are fainter than the PLR of shorter period Mira variables due to the circumstellar extinction. (Whitelock et al. 1991; Glass et al. 1995; Matsunaga et al. 2009). For example, the K_s band PLR shows a large scatter with many long-period Mira variables getting fainter (Ita & Matsunaga 2011). In

* Released on 2019 October 4th.

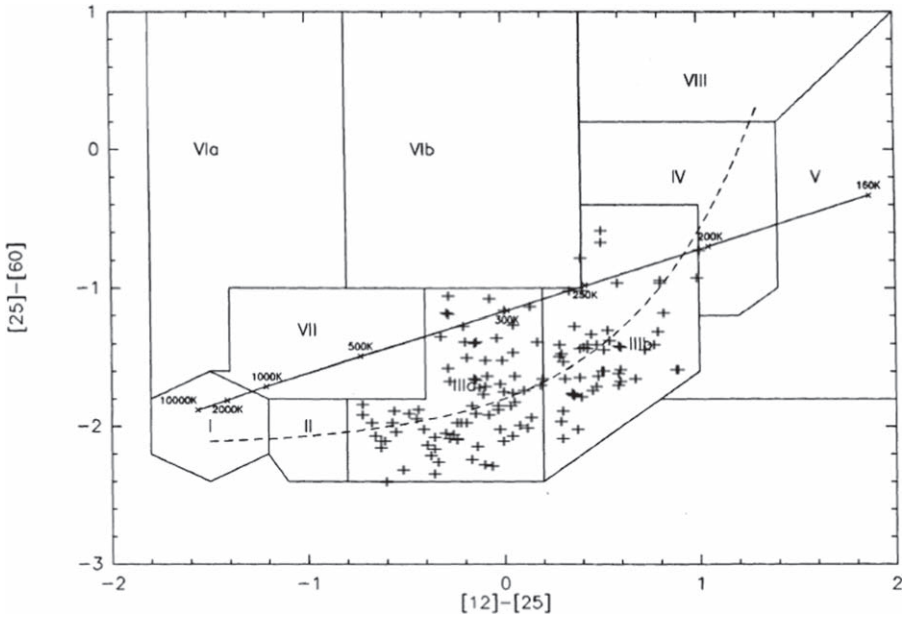

Figure 1. Distribution of 108 sources for which we determined their periods in this paper, on the *IRAS* color−color diagram. The solid lines correspond to the border lines of regions indicated in van der Veen & Habing (1988).

contrast, the 3.6 μm PLR of Mira variables for the Large Magellanic Cloud (LMC) presented in the same paper has a much tighter relation which would be more useful for determining the distances of longer period Mira variables. In the present paper, we report an analysis of the monitoring data in the near-infrared K' band, and derived parameters for 108 Mira variables. We selected Mira variable candidates from the *IRAS* point-source catalog (PSC), to isolate long-period candidates which are typically young in the IIIa and IIIb regions of the *IRAS* color–color diagram (van der Veen & Habing 1988). We combined these observations with the 2MASS data and the *Wide-field Infrared Survey Explorer* (*WISE*) data, to determine the spatial distribution of long-period Mira variables and compare them with the spiral arm structure.

2. Sample Selection and Observation

2.1. Sample Selection

We selected bright infrared sources that satisfy the following criteria as candidates of the long-period Mira variables from the *IRAS* PSC (Neugebauer et al. 1984). First, sources with decl. $> -25°$ were selected considering the latitude of our observatory site, Kagoshima, located at a latitude of 31°.5 north. Second, targets needed to be bright in all bands; 12, 25, and 60 μm (flux density quality = 3 in the *IRAS* PSC). Third, targets are required to be located in the IIIa or IIIb regions on the *IRAS* color–color diagram (van der Veen & Habing 1988). The position of the IIIa and IIIb regions are indicated in Figure 1, together with the distribution of the 108 Mira variables examined in this paper. The IIIa and IIIb regions lie around the most evolved phase of the sequence of dust shell evolution of AGB (van der Veen & Habing 1988). Therefore, the stars located in these regions are likely to have a longer period. There are 2300 for the IIIa and 280 for IIIb, which satisfy the above three criteria.

Figure 2 shows the $l - b$ diagram of sources satisfying the criteria including those for which we report distances in this paper. There is a gap around $l = 80°$. There are few *IRAS* sources in this area because *IRAS* observation was not performed in this area. In this paper, we report on 108 sources for which accurate periods were determined so far.

2.2. Observation

Our monitoring observations were carried out at Iriki observatory operated by Kagoshima University (Chibueze et al. 2016), Japan, since 2003. A near-IR camera with a 512 × 512 HgCdTe array detector attached to a 1 m telescope yielding 5′.38 × 5′.38 field of view (0″.63 pixel scale) was used. The typical seeing measurement at the Iriki observatory is 1″.5. Monitoring observations in the K' band were performed in the fields centered on the position of the selected *IRAS* sources. Each set of observations consists of five exposures at slightly dithered positions with an exposure time of 1–12 s. We adjusted the exposure time depending on the sky background level, and the brightness of the target and reference stars in the same field. Stars brighter than $K' \sim 6.5$ mag would be saturated at the best focus position, and therefore we observed such bright sources with the focus off. For targets for which no reference star was found in the same field of view, we also observed the standard stars listed in Elias et al. (1982) on the same night. We searched for the counterparts of *IRAS* objects in the 2MASS image. In many cases, the bright near-infrared counterparts were found near the *IRAS* position. The coordinates of the 108 sources in Table 1 are based on the 2MASS catalog (J2000.0).

3. Data Reduction

3.1. Image Reduction

Raw images were reduced using our automatic image reduction pipeline that utilizes tasks from IRAF. The procedure has five main steps as follows. First, dark images were subtracted from the raw image to remove the effect of dark current. Dark current subtraction was made using the 3σ clipping of a combination of 10 dark frames with exposure times equal to those of the observations carried out on the same

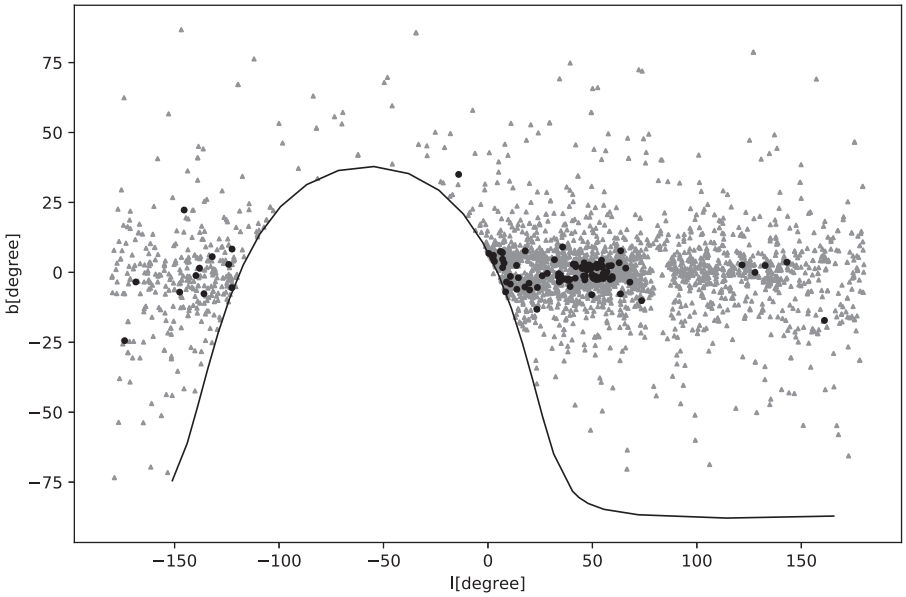

Figure 2. The $l - b$ distribution of the *IRAS* sources. Gray marks (triangle) indicate all the sources that satisfy our criteria. Black marks are the sources for which we determined their distance in this paper. The solid line corresponds to decl. $= -25°$.

nights as the observed targets. Second, we standardized the raw image using a flat field to correct for the nonuniformity of sensitivity of our detector. Flat fields were obtained using twilight-flats from 2003 to 2012. From 2013, operations moved to using dome-flats. We obtained 10–30 images of them every week and calculated the average of difference between on-flat and off-flat. Third, we performed sky subtraction to reduce the fixed pattern of the raw images due to foreground or background radiation. The sky-frame was subtracted from the raw image after standardization to correct for the sky value. We calculated the sky value from starless area. For the on-focus images, we subtract the self-sky images, which were a median combined image without positional-shift. The blank sky fields adjacent to the target field were observed separately for out of focus images, and their median combined images were also made using the same approach as that used for the on-focus images. Fourth, we combined the slightly dithered images into a single image. We measure the (x, y) position of the same stars in the dithered images. We calculated the positional shifts among the dithered images. We combined them using the *imcombine* task in IRAF based on the above information. Fifth, we inserted the World Coordinate System (WCS). We obtained astrometric solutions by comparing detected stars with the 2MASS PSC (Skrutskie et al. 2006) and then inserted the WCS into the FITS file. We searched for the counterparts of the stars in our images in the 2MASS PSC. Pixel coordinates (x, y) of the detected sources were converted to equatorial coordinates (R.A., decl.) using a linear transformation. The equatorial coordinates were based on the International Celestial Reference System via the 2MASS-PSC.

3.2. Photometry

We performed aperture photometry for the Mira candidates and reference stars on the same images with the APPHOT package in IRAF. For each image, reasonably bright stars with variation of less than 0.1 mag were used as reference stars. The instrumental magnitude was calibrated by comparing them to the 2MASS PSC using reference stars. For the images without any reference stars in the same field or defocused images, we calibrated the target using the standard stars in Elias et al. (1982).

4. Results

4.1. Light Curve

We performed a period search employing a least-square method to fit sinusoidal curves to the photometric measurements of all samples in our monitoring survey. The light curve of IRAS 18511-1041 is illustrated in Figure 3 as an example and those for all the sources are given as online material. We fit our photometric data to the following equation,

$$m = B + (A/2)\sin(2\pi t/P + \phi) \quad (1)$$

where m is the observed magnitude, B is the center value of the sinusoidal, A is the peak to peak amplitude, P is the period, t is Modified Julian Date (MJD), and ϕ is the phase at $t = 0$.

We searched for a period that minimizes the rms residual with a search window of 100–1500 days. Then we visually inspected the folded light curve, the fitted sinusoid and photometric data plotted against phase. As a result, we determined the period for 108 sources (Table 1). In addition, we use the average of the matching sinusoidal curve (B in Equation (1)) as the mean magnitude.

4.2. Period Distribution

A histogram of the derived periods of our monitoring samples is given in Figure 4, which shows a peak between 500 and 600 days. Generally, populations of Mira variables peak at around 300 days, but our Mira candidate population shows a peak at around 500 days. This is as expected because our samples selected from the IIIa and IIIb regions of the *IRAS* color–color diagram. As explained in van der Veen & Habing (1988) the various regions of the *IRAS* color–color diagram host stars at different evolutionary stages and mass ejections;

Table 1
Observable Characteristics of Our Samples

IRASname	R.A. [h m s] (J2000)	Decl. [d m s] (J2000)	Period (days)	Amplitudes (Kmag)	K'(mag)	W1 (mag)	Aw1 (mag)	Distance (kpc)	Z (kpc)
IRAS 00361+6515	00 39 03.61368	+65 32 07.2204	650	1.89	9.75	6.36	0.28	14.42	0.68
IRAS 01304+6211	01 33 51.21048	+62 26 53.2032	759	1.18	6.90	3.83	0.19	5.37	0.00
IRAS 02173+6322	02 21 11.90064	+63 36 18.2196	698	1.68	8.28	5.91	0.14	13.29	0.57
IRAS 03385+5927	03 42 39.99072	+59 36 59.9652	618	1.93	7.43	3.79	0.14	4.50	0.28
IRAS 03453+3207	03 48 32.31240	+32 16 43.7916	409	1.02	4.36	3.54	0.06	2.87	−0.85
IRAS 04312+1007	04 33 58.38048	+10 13 52.6872	425	0.57	4.10	3.44	0.04	2.86	−1.18
IRAS 05552+1720	05 58 07.50696	+17 20 58.4772	520	1.04	5.88	4.58	0.10	5.64	−0.34
IRAS 06228-0244	06 25 21.64896	−02 46 37.9128	412	1.15	4.68	3.98	0.05	3.56	−0.44
IRAS 06418-1317	06 44 08.23968	−13 20 08.9232	347	0.88	6.39	6.15	0.05	8.27	−1.10
IRAS 06583-0655	07 00 44.51832	−06 59 43.5984	431	0.97	4.60	4.21	0.11	4.00	−0.08
IRAS 07109-0713	07 13 23.20944	−07 18 33.6708	316	1.30	6.93	5.82	0.07	6.47	0.17
IRAS 07153-2411	07 17 28.17912	−24 17 13.5852	495	2.06	5.38	3.89	0.03	4.05	−0.39
IRAS 07372-1036	07 39 39.53064	−10 43 05.4588	467	0.86	4.36	3.76	0.02	3.65	0.36
IRAS 07434-1847	07 45 40.92408	−18 54 29.1744	678	1.39	11.51	5.59	0.05	11.67	0.58
IRAS 08066-1719	08 08 56.45328	−17 28 38.8452	510	1.57	6.97	3.73	0.01	3.89	0.56
IRAS 08116+0843	08 14 18.76224	+08 34 24.4704	263	0.96	4.65	4.65	0.00	3.31	1.26
IRAS 15106-1532	15 13 25.77504	−15 43 59.5416	268	1.38	8.66	7.25	0.01	11.07	6.35
IRAS 17179-2452	17 21 01.47744	−24 55 50.1492	597	2.03	10.64	6.93	0.15	18.38	2.17
IRAS 17259-2326	17 28 59.79696	−23 28 38.9676	648	1.90	8.17	5.77	0.19	11.39	1.20
IRAS 17287-1955	17 31 40.98336	−19 58 07.7268	562	2.01	10.37	6.86	0.17	16.71	2.16
IRAS 17292-2408	17 32 16.53480	−24 10 56.6256	682	2.02	7.95	5.55	0.19	10.78	0.95
IRAS 17304-1933	17 33 22.14840	−19 35 52.2348	547	1.46	7.60	5.72	0.15	9.73	1.24
IRAS 17324-1918	17 35 23.78904	−19 20 47.0508	610	1.40	8.15	5.16	0.10	8.49	1.04
IRAS 17350-2413	17 38 08.84976	−24 14 49.2756	542	2.46	10.63	7.14	0.16	18.46	1.25
IRAS 17411-2029	17 44 04.88088	−20 30 32.2920	561	2.48	9.25	6.06	0.15	11.66	0.95
IRAS 17476-2036	17 50 35.63016	−20 37 43.6152	432	1.44	8.42	6.24	0.22	9.72	0.56
IRAS 17521-2201	17 55 07.46544	−22 01 31.6128	850	3.24	12.45	7.69	0.27	33.87	1.01
IRAS 17531-0940	17 55 53.14608	−09 41 20.6448	682	2.34	7.34	4.68	0.16	7.33	0.98
IRAS 18033-1551	18 06 12.86976	−15 51 06.3072	475	1.56	8.48	6.38	0.27	11.04	0.48
IRAS 18117-2022	18 14 42.51720	−20 21 10.2060	633	2.20	8.49	4.85	0.39	6.67	−0.17
IRAS 18154-2257	18 18 30.18408	−22 56 01.3704	708	2.06	8.40	6.12	0.13	14.96	−0.90
IRAS 18211-1712	18 24 05.21208	−17 11 13.8048	457	1.86	8.31	5.14	0.21	6.18	−0.21
IRAS 18216+0634	18 24 03.72288	+06 36 25.8984	830	2.04	8.70	5.19	0.03	11.73	1.85
IRAS 18219-2140	18 24 57.70008	−21 38 51.4900	703	2.23	9.86	5.091	0.09	9.40	−0.69
IRAS 18282-2458	18 31 19.11480	−24 56 08.0160	394	0.98	9.47	6.60	0.06	11.38	−1.38
IRAS 18307+0102	18 33 15.25128	+01 04 39.0828	494	1.19	6.15	4.65	0.30	5.07	0.40
IRAS 18351-1947	18 38 08.97120	−19 44 28.2300	494	1.34	4.83	4.02	0.06	4.25	−0.45
IRAS 18382-1338	18 41 04.72152	−13 35 52.0044	676	1.73	8.30	5.60	0.17	11.04	−0.75
IRAS 18394-1600	18 42 22.31184	−15 57 05.6988	489	1.31	7.09	4.83	0.08	6.06	−0.55
IRAS 18404-0645	18 43 07.20960	−06 42 40.1400	760	2.15	7.11	4.00	0.13	5.98	−0.13
IRAS 18418-0415	18 44 31.32792	−04 12 15.8724	897	2.11	8.30	5.41	0.28	12.39	−0.08
IRAS 18475-1428	18 50 22.90104	−14 24 30.7332	590	2.20	7.90	6.15	0.10	13.03	−1.43
IRAS 18511-1044	18 53 56.07672	−10 40 40.8072	647	1.86	8.95	5.85	0.07	12.48	−1.17
IRAS 18522+0032	18 54 45.59952	+00 36 02.1528	700	2.09	8.64	5.32	0.55	8.44	−0.07
IRAS 18530+0817	18 55 25.22304	+08 21 15.9300	745	1.47	4.96	3.41	0.30	4.13	0.21
IRAS 18549+0905	18 57 20.81592	+09 09 40.8816	471	0.95	4.66	4.02	0.21	3.78	0.19
IRAS 18556+0003	18 58 14.96976	+00 07 28.5996	643	1.87	8.87	6.07	0.31	12.33	−0.31
IRAS 18559+0103	18 58 31.76232	+01 07 47.4672	771	2.31	12.78	7.50	0.27	28.50	−0.53

Table 1
(Continued)

IRASname	R.A. [h m s] (J2000)	Decl. [d m s] (J2000)	Period (days)	Amplitudes (Kmag)	K'(mag)	W1 (mag)	Aw1 (mag)	Distance (kpc)	Z (kpc)
IRAS 18567+0003	18 59 21.17376	+00 07 26.4324	667	1.37	5.60	4.25	0.25	5.67	−0.17
IRAS 18585+0900	19 00 53.82114	+09 05 02.7305	867	1.59	5.80	3.27	0.29	4.48	0.16
IRAS 19010+1307	19 03 21.50832	+13 12 01.2024	843	2.48	8.20	5.87	0.18	15.16	0.90
IRAS 19026+0007	19 05 15.99624	+00 12 18.5652	482	1.25	5.37	4.46	0.12	4.95	−0.26
IRAS 19031-0035	19 05 40.52520	−00 30 45.6120	321	1.18	9.52	6.84	0.11	10.31	−0.61
IRAS 19037+0204	19 06 18.45264	+02 09 03.5280	580	0.86	5.95	5.18	0.24	7.67	−0.31
IRAS 19046+1121	19 07 01.79688	+11 26 10.6692	526	2.26	10.34	6.22	0.22	11.46	0.36
IRAS 19068+1127	19 09 11.67960	+11 32 48.1956	678	1.40	5.40	4.54	0.22	6.64	0.16
IRAS 19074+0336	19 09 54.92112	+03 41 27.3912	612	1.37	7.36	4.70	0.18	6.67	−0.28
IRAS 19082+1456	19 10 33.33888	+15 01 11.6616	464	1.46	6.41	5.30	0.15	6.96	0.32
IRAS 19087+0323	19 11 17.00856	+03 28 24.3984	631	1.94	7.39	4.97	0.35	7.18	−0.35
IRAS 19087+1413	19 11 05.30352	+14 18 23.0328	536	0.89	5.14	4.04	0.09	4.55	0.18
IRAS 19097+0411	19 12 13.21704	+04 16 54.5664	517	1.21	5.82	4.44	0.25	4.90	−0.23
IRAS 19126+0648	19 15 06.06960	+06 53 29.0256	630	2.09	11.04	6.87	0.23	18.15	−0.66
IRAS 19128+1310	19 15 07.96872	+13 16 00.0552	817	3.43	8.38	4.79	0.26	8.64	0.13
IRAS 19131+1551	19 15 25.06176	+15 56 32.8848	851	2.81	11.41	5.41	0.20	12.27	0.44
IRAS 19136+2055	19 15 47.39376	+21 00 32.5116	589	1.78	9.14	6.13	0.18	12.42	0.94
IRAS 19143+1817	19 16 33.90949	+18 22 51.9676	415	0.95	4.04	3.52	0.15	2.76	0.14
IRAS 19149+1638	19 17 11.55675	+16 43 54.6222	583	1.49	5.16	3.54	0.20	3.69	0.13
IRAS 19151+1456	19 17 26.10720	+15 01 59.0268	534	1.25	5.88	4.87	0.19	6.35	0.13
IRAS 19167+1733	19 19 00.02040	+17 38 51.9036	497	0.88	5.48	4.35	0.29	4.47	0.16
IRAS 19175+1042	19 19 57.26616	+10 48 09.1440	545	1.64	7.93	5.13	0.31	6.87	−0.16
IRAS 19176+1939	19 19 48.03696	+19 45 35.8776	560	1.31	6.44	5.50	0.21	8.76	0.44
IRAS 19186+0315	19 21 11.69976	+03 20 57.8652	497	1.82	6.15	4.65	0.12	5.55	−0.49
IRAS 19190+1128	19 21 26.68848	+11 33 56.6100	856	2.42	7.60	4.02	0.25	6.36	−0.14
IRAS 19190+3035	19 20 59.23344	+30 41 28.6764	581	1.58	8.23	5.47	0.38	8.28	1.11
IRAS 19195-1423	19 22 22.58256	−14 18 05.0688	425	1.36	6.42	4.75	0.03	5.26	−1.20
IRAS 19195+1747	19 21 44.11944	+17 53 09.7080	519	1.07	5.02	3.74	0.29	3.52	0.10
IRAS 19202+2009	19 22 25.53000	+20 15 35.4528	782	1.54	5.90	4.43	0.22	7.18	0.33
IRAS 19235+1034	19 25 56.66640	+10 40 22.8864	540	1.29	8.07	6.99	0.18	17.13	−0.80
IRAS 19236+2003	19 25 49.34208	+20 09 13.4424	552	1.67	6.29	4.56	0.22	5.59	0.18
IRAS 19237+1430	19 26 02.24328	+14 36 39.2760	559	1.24	4.93	3.81	0.26	3.92	−0.06
IRAS 19261+1435	19 28 28.48488	+14 41 52.1592	633	1.80	7.95	5.97	0.41	11.09	−0.25
IRAS 19276+1500	19 29 53.85312	+15 06 48.3912	551	1.28	6.18	5.02	0.27	6.73	−0.17
IRAS 19282+2253	19 30 19.90704	+23 00 01.0224	639	1.25	5.15	4.07	0.12	5.31	0.21
IRAS 19283+1421	19 30 38.02152	+14 27 55.7568	468	1.39	5.94	4.06	0.24	3.78	−0.12
IRAS 19303+1553	19 32 35.87520	+15 59 41.0712	637	1.11	7.30	6.14	0.28	12.82	−0.35
IRAS 19305+2410	19 32 39.94416	+24 16 55.9272	685	1.06	5.14	4.30	0.16	6.18	0.26
IRAS 19307+1441	19 33 04.51344	+14 48 27.2628	574	0.95	6.14	5.37	0.25	8.27	−0.32
IRAS 19320+2013	19 34 14.17824	+20 20 02.3856	523	1.13	5.83	4.47	0.30	4.90	0.02
IRAS 19333+1918	19 35 30.77928	+19 25 06.4812	630	1.39	4.86	3.87	0.29	4.43	−0.04
IRAS 19338+1522	19 36 10.28304	+15 28 47.8596	303	0.99	5.06	4.56	0.16	3.36	−0.15
IRAS 19344+2114	19 36 37.25640	+21 21 13.6728	474	1.99	6.67	4.79	0.29	5.22	0.02
IRAS 19347+2755	19 36 44.55072	+28 01 58.3428	632	1.63	7.21	5.95	0.11	12.57	0.75
IRAS 19349+1657	19 37 12.79200	+17 03 47.3832	543	1.26	6.52	4.77	0.19	6.13	−0.21
IRAS 19352+1914	19 37 26.17152	+19 20 54.2472	862	1.42	6.20	4.07	0.21	6.67	−0.11
IRAS 19352+2030	19 37 23.99712	+20 36 57.8088	523	1.18	8.89	5.13	0.26	6.77	−0.04
IRAS 19359+1936	19 38 12.46848	+19 43 08.8104	581	1.23	8.91	6.75	0.37	14.91	−0.24

Table 1
(Continued)

IRASname	R.A. [h m s] (J2000)	Decl. [d m s] (J2000)	Period (days)	Amplitudes (Kmag)	K'(mag)	W1 (mag)	Aw1 (mag)	Distance (kpc)	Z (kpc)
IRAS 19360+1629	19 38 16.68024	+16 36 13.7880	492	1.21	5.13	4.04	0.12	4.15	−0.18
IRAS 19361+1805	19 38 20.20944	+18 12 38.5848	592	1.34	6.35	5.53	0.20	9.34	−0.27
IRAS 19395+1827	19 41 44.55456	+18 34 25.8060	502	1.49	6.04	4.77	0.16	5.81	−0.22
IRAS 19395+1949	19 41 43.42344	+19 56 31.6644	560	1.26	5.42	4.06	0.15	4.63	−0.12
IRAS 19462+2232	19 48 26.23536	+22 39 56.8404	494	1.36	5.70	4.17	0.22	4.22	−0.11
IRAS 19479+2111	19 50 07.30704	+21 19 04.2456	477	0.92	4.38	3.89	0.09	3.81	−0.17
IRAS 19486+2215	19 50 48.45816	+22 23 13.3008	515	1.15	5.47	5.04	0.18	6.67	−0.25
IRAS 19490+1049	19 51 24.95328	+10 57 22.1364	562	2.35	9.01	6.21	0.04	13.16	−1.83
IRAS 19494+2939	19 51 29.96712	+29 47 27.6504	442	0.33	9.20	6.32	0.20	10.34	0.27
IRAS 20137+2838	20 15 47.65440	+28 47 54.9168	531	1.06	7.10	5.96	0.20	10.36	−0.63
IRAS 20181+2234	20 20 21.92136	+22 43 48.4788	550	1.44	7.06	4.68	0.07	6.27	−0.84
IRAS 20531+2909	20 55 17.68320	+29 20 50.7804	346	0.97	7.83	5.92	0.02	7.51	−1.32

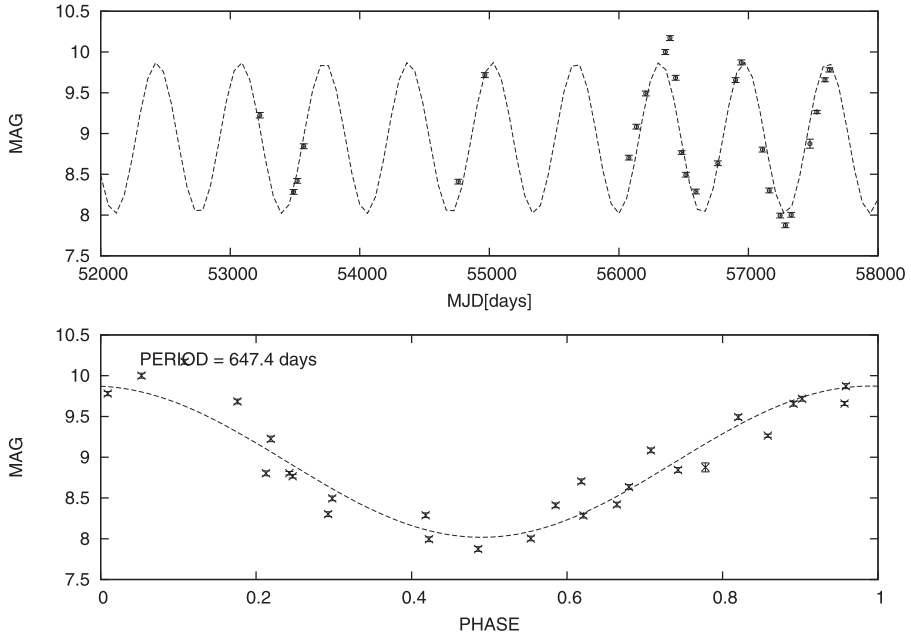

Figure 3. (Top) The apparent K' magnitude of IRAS 18511-1041 against MJD as an example of our monitoring observation. (Bottom) The folded light curve of IRAS 18511-1041. The dotted line is the best-fit sine curve to data points.

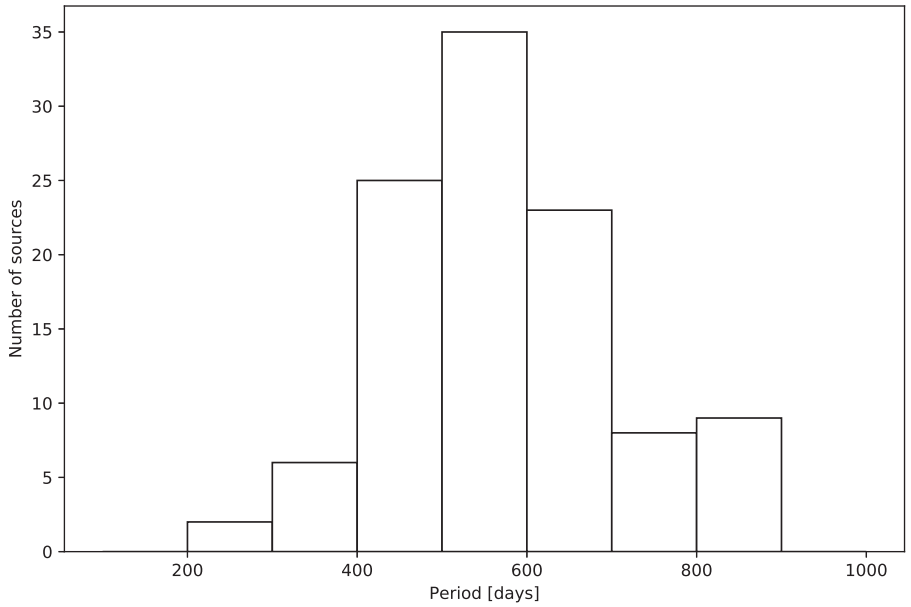

Figure 4. Period histogram of Mira variables for which we determined their period.

the stars belonging to IIIa and IIIb have more developed dust shells. Therefore, we were able to demonstrate that the stars located in these groups have longer periods.

Another period distribution of long-period Mira variables in the Galactic bulge is given in Whitelock et al. (1991), whose sample was also selected from the *IRAS* point-source catalog although the selection criteria was different from ours. Their population of Mira variables had a peak at around 400 days. Therefore our sample represents a population of Mira variables that have longer periods than typical Mira variables and the sample of Whitelock et al. (1991). We found that the selection of sources in the IIIa and IIIb regions is a good method to isolate longer period Mira variables, which most likely have large initial masses.

4.3. Amplitude Distribution

There are two types of long-period variables; Mira variables and semi-regular (SR) variables, and our 108 Mira candidates could be contaminated by SR variables. While both classes of variables can have similar periods, their pulsation amplitudes typically differ. Mira variables typically have pulsation amplitudes of $K' > 0.4$ mag, while SR variables typically have smaller amplitudes of $K' < 0.4$ mag (e.g., Whitelock et al. 2000). Using this criterion we inspected the pulsation amplitudes of the Mira candidates, which are shown in Figure 5. The amplitude of IRAS 19494+2939 is too small to support the classification as a Mira variable, and this object is not included in the following discussions. The longer period Mira variables have larger amplitudes. To further test the

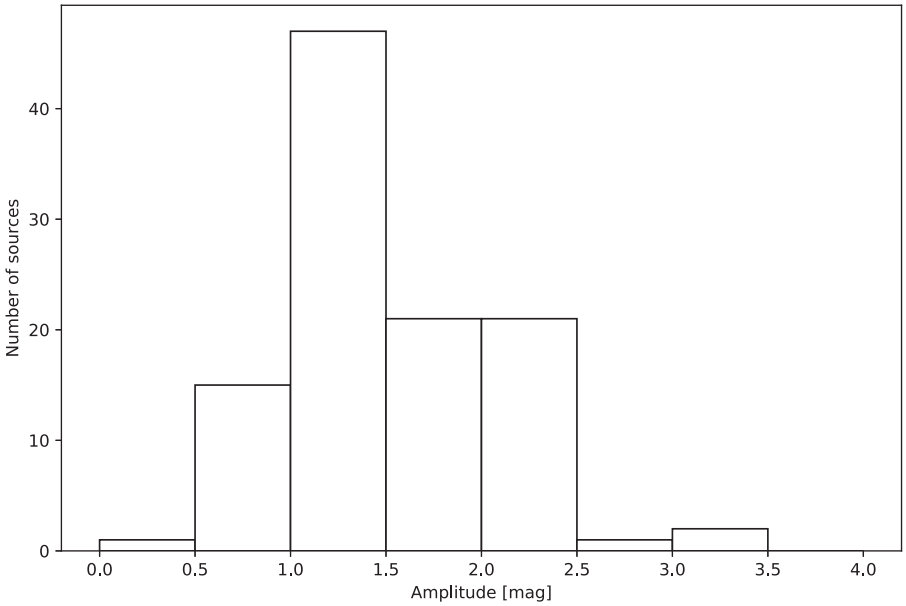

Figure 5. Amplitude histogram of Mira variables for which we determined their amplitude in this paper.

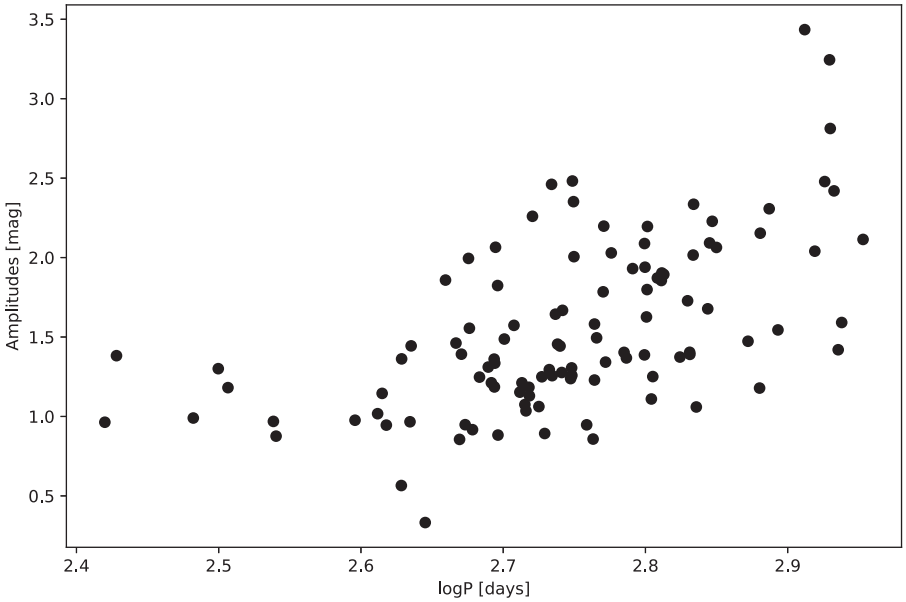

Figure 6. Period–amplitude diagram.

validity of our Mira candidates selection we plotted K' band amplitudes against periods (Figure 6). As expected, the Mira candidate population shows a correlation; longer periods for larger pulsation amplitudes.

5. Distance Determination

5.1. Period–Luminosity Relation

The PLR of Mira variables was first established in the LMC and a recent evaluation of the PLR in the LMC was given in Ita & Matsunaga (2011). Since the PLR enables prediction of a star's absolute magnitude it is possible to calculate the distance modulus of Mira variables by combining measurements of the pulsation period and an extinction corrected apparent magnitude. We aim to estimate the distances of our long-period Mira variables using the PLR to reveal their distribution in our galaxy. The PLR of Mira variables at infrared wavelengths is a useful tool for distance determination within the Milky Way and at larger distances, since there is less extinction at these wavelengths.

The PLR at shorter wavelengths becomes imprecise for Mira variables with periods longer than about 300 days. C-rich Mira variables locate below the extension of the PLR along the period in the optical and JHK_s bands (Ita & Matsunaga 2011). On the other hand, O-rich Mira variables with longer periods locate above the same extended PLR in the optical and JHK_s bands. Some O-rich Mira variables with very long periods ($\log P > 3.0$) are found below the extended PLR, probably due to circumstellar extinction, similarly to the C-rich Mira variables in the same paper. As a result of these deviations, the PLR at the K band or shorter wavelengths cannot be reliably used for the determination of distances. On the contrary, the 3.6 μm PLR in

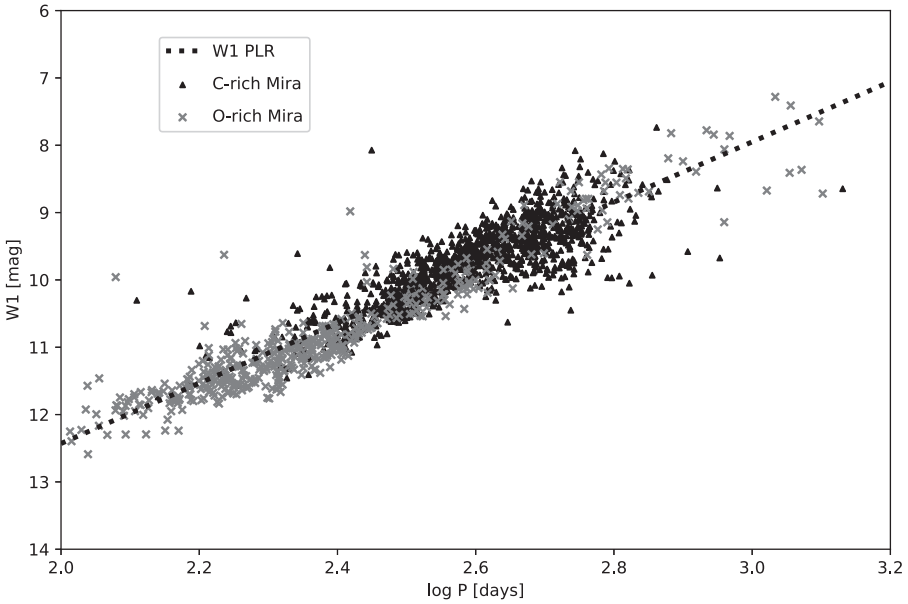

Figure 7. 3.4 μm (W1) period–luminosity relation in the LMC. Gray points (cross) are O-rich Mira variables from the OGLE-III catalog. Black points (triangles) are C-rich Mira variables. Dotted line is the best-fit line of the least-square fitting for both O-rich and C-rich Mira variables.

the same paper shows a tight and linear relation for both short and long-period members in the *Spitzer* 3.6 μm band, although it is based on single epoch data. This suggests that circumstellar extinction does not severely affect the PLR of longer period Mira variables at around 3 μm and thus can be used to more reliably determine distances.

In this paper, we combine the pulsation period of our monitoring observations we determined for the 108 long-period Mira variables with magnitudes from *WISE* (Wright et al. 2010) band *I* (3.4 μm) to estimate the distances to our sample via the 3.4 μm PLR. Our methodology is to first establish the 3.4 μm PLR. Second, we derive the interstellar extinction at 3.4 μm using a 3D reddening map. Finally, we derive the interstellar extinction corrected 3.4 μm magnitudes from the *WISE* data and use these to derive distance moduli for our sample.

In the present case, *WISE* is preferable to *Spitzer* since the latter does not contain data for all of our sources.

5.2. The PLR at 3.4 μm

To establish the PLR at 3.4 μm we use the photometries of 1663 Mira variables in the LMC, for which the periods were determined by OGLE-III (Soszyński et al. 2009). Since these sources are located in the LMC, we assume they reside equidistantly and the distance modulus of the LMC is 18.5. Figure 7 shows the apparent magnitudes of W1 from ALLWISE (Cutri et al. 2014) against their period for 1663 Mira variables listed in the OGLE-III catalog. We can see no significant difference in the distribution between C-rich and O-rich Mira variables. We performed least-square fitting to all sources regardless of C-rich and O-rich with a linear function. A least-square fitting to these data produces the following relation.

$$m_{W1} = -4.48 \pm 0.05 \times \log P + 21.39 \pm 0.13 \quad (2)$$

$$M_{W1} = -4.48 \pm 0.05 \times \log P + 2.89 \pm 0.13, \quad (3)$$

where M_{W1} is the absolute magnitude converted by the distance modulus of the LMC, and m_{W1} is the apparent magnitude in W1. Figure 8 is a histogram of the residual from the best-fit

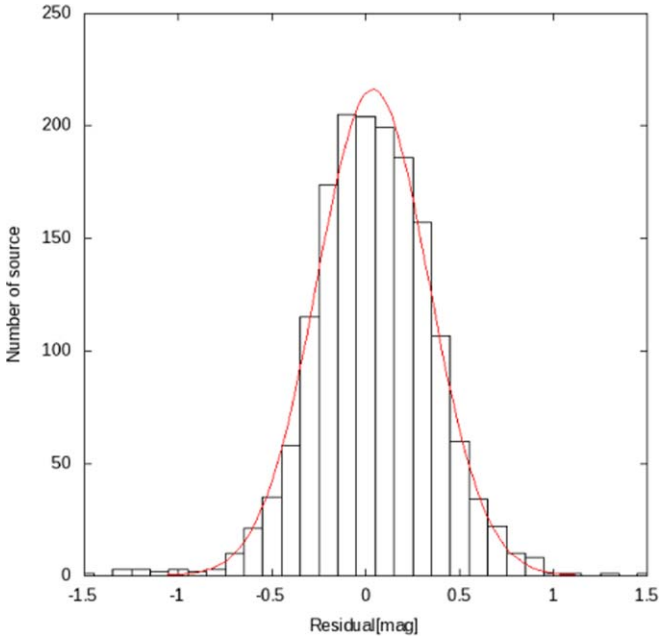

Figure 8. Histogram of the fitting of data points from the best-fit line. The red line shows the curve determined by applying a Gaussian filter.

PLR. We use the width of the Gaussian, $\sigma = 0.29$ mag, as an error source in the following analysis. The 3.4 μm PLR is likely due to the balance of extinction and thermal radiation of circumstellar dust, and the two cases; Mira variables with and without the circumstellar dust, share the same position in the PL diagram.

Riebel et al. (2010) also reported the 3.6 μm PLR of Mira variables in LMC using a similar data set, the MACHO (MAssive Compact Halo Objects survey) and the *Spitzer* SAGE catalog. They obtained the equations of PLR for the O-rich and C-rich Mira variables separately as well as for all sources including both the O-rich and C-rich Mira variables. The PLRs of O-rich and C-rich Mira variables give $m_{W1} = 9.683$ mag and

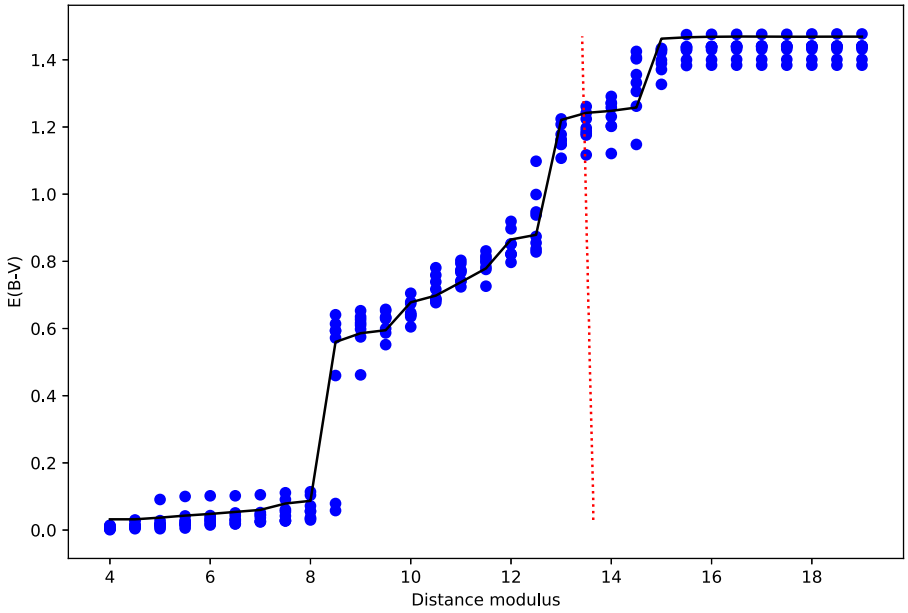

Figure 9. $E(B-V)$ against the distance modulus based on the 3D reddening map for the direction toward IRAS 01304+6211. Blue points: $E(B-V)$ from the 3D reddening map. Black line: the best-fit line of blue points provided by the 3D reddening map. Dotted red line: Equation (4) of IRAS 01304+6211.

9.171 mag at $\log P = 2.7$, and they differ from our relation (Equation (2)) by 0.123 mag and 0.389 mag, respectively. The PLR of all the sources replies $m_{W1} = 9.156$ mag at $\log P = 2.7$ and their PLR differs from our relation (Equation (2)) by 0.138 mag. The difference for all the sources PLR is smaller than the residual of our fitting and is not significant considering the slight difference of wavelength (3.4 μm or 3.6 μm) and the difference of fitting range of period. In this paper, our purpose is to obtain distances for long-period Mira variables in Milky Way and so it is difficult to classify as O-rich or C-rich correctly for our samples and hence difficult to apply the PLR dedicated to the O-rich or C-rich Mira variables even if we know the equations of PLR for C-rich and O-rich separately. Therefore, we use our equation of PLR obtained from both C-rich and O-rich without discrimination in this paper.

5.3. Distance Modulus for Our Sources and Interstellar Extinction of Our Sample at 3.4 μm

We estimate distances to Mira variables using the 3.4 μm PLR. The apparent distance modulus at 3.4 μm is related to the true distance modulus μ and the extinction A_{W1} at 3.4 μm as follows.

$$\mu = m_{W1} - M_{W1} - A_{W1} = \mu_0 - A_{W1} \quad (4)$$

Here, μ_0 ($=m_{W1} - M_{W1}$) is the apparent distance modulus without correction of interstellar extinction. Our sample, consisting of longer period Mira variables, resides in the Galactic plane. Thus, corrections must be derived for interstellar extinction at 3.4 μm as described below.

We determined A_{W1} using a 3D map of interstellar dust reddening, covering three-quarters of the sky (decl. $> -25°$) out to a distance of several kiloparsecs. (see http://argonaut.skymaps.info/; Green et al. 2018, 2015) They determined the interstellar reddening ($E(B-V)$) as a function of distance modulus for each line of sight using 800 million stars from Pan-STARRS 1 and 2MASS. Here, we use a universal dust extinction law with $R(V) = 3.1$ and $A_{L\text{-band}}/E(B-V) = 0.157$ to convert $E(B-V)$ to A_{W1} (Schlafly & Finkbeiner 2011). On the other hand, interstellar extinction increases against distance modulus and A_{W1} is expressed as a monotonically increasing function ($f(\mu)$) of μ. This function is provided as the "best-fit line" from the 3D reddening map. We can estimate the interstellar extinction and the distance modulus by solving the simultaneous equations of Equation (4) and $f(\mu)$. We show an example for IRAS 01304+6211 in the Figure 9. We used an error shown in the 3D reddening map. We summarize the A_{W1} values, the line-of-sight distances (D), and the height distances (z) in Table 1. We estimated the errors of μ using the error of PLR, the error of A_{W1} and the *WISE* photometric error.

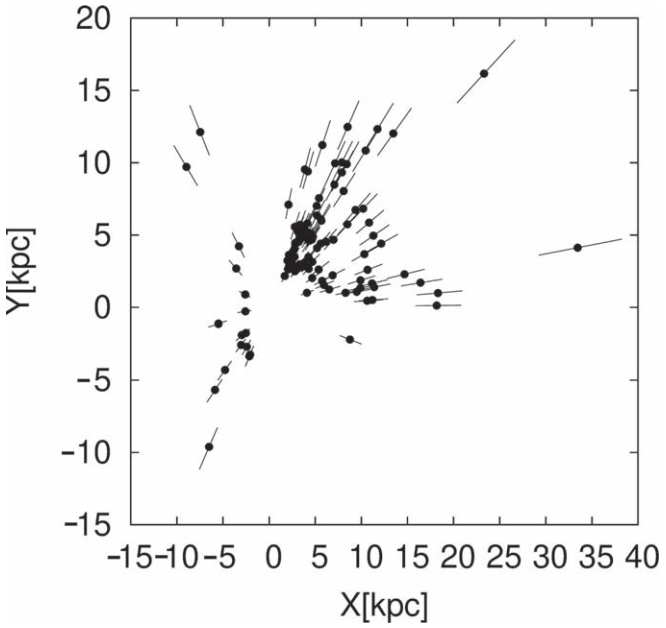

Figure 10. Galactic face-on distribution of all Mira variables for which we determined their distance in this paper. The Galactic center is at (8, 0) and the Sun is at (0, 0).

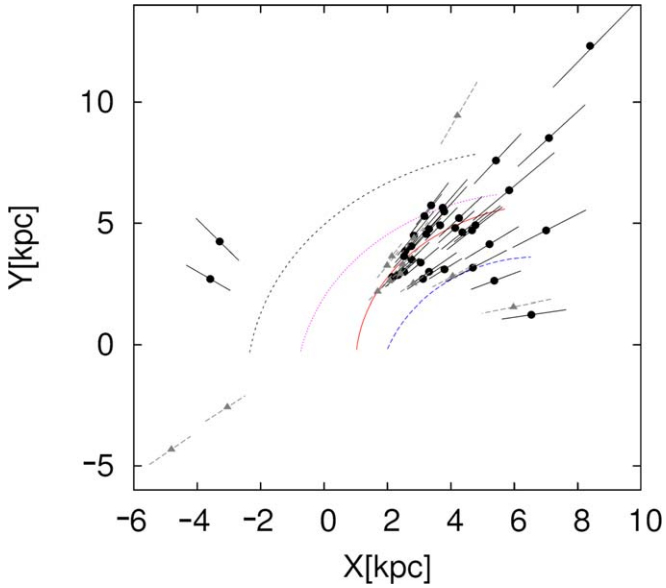

Figure 11. Galactic face-on distribution of our sample in the thin disk ($|Z| < 0.3$ kpc). Black circle points: the sources located in $|Z| < 0.3$ kpc with the periods of $\log P > 2.7$. Gray triangle points: the sources in $|Z| < 0.3$ kpc with the periods of $\log P < 2.7$. The Galactic center is at (8, 0) and the Sun is at (0, 0). The distribution of HMSFR is sorted into individual arms which are represented by colors, Scutum arm, blue; Sagittarius arm, red; Local arm, violet; Perseus arm, black.

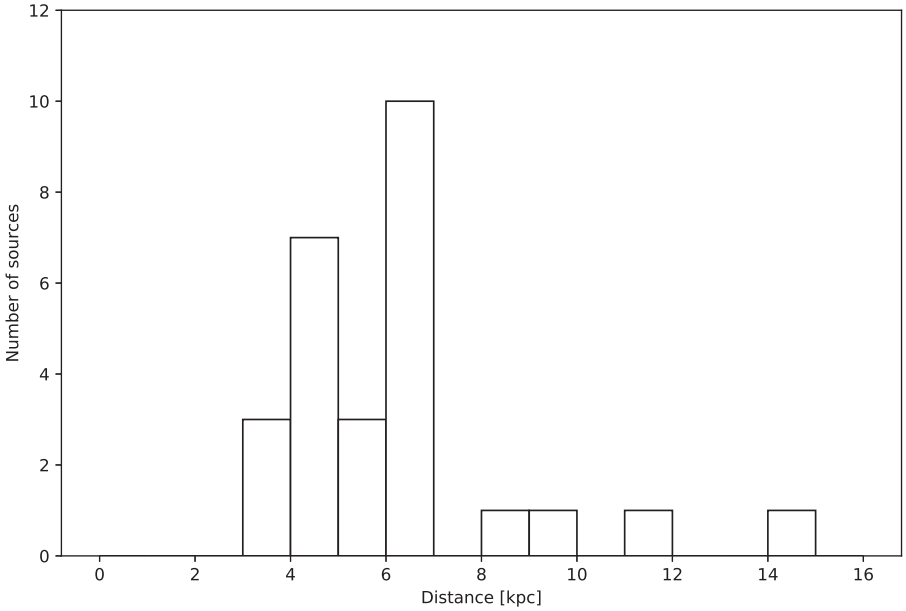

Figure 12. Histogram of the sources located in $|Z| < 300$ pc and $40° < l < 60°$.

6. Discussion

6.1. Face-on Distribution

Based on the distances derived from our monitoring survey we illustrate the Galactic face-on distribution of all of our Mira variables in Figure 10. To investigate the possibility that longer period Mira variables are associated with the spiral arm structures in the Milky Way, we compare our sample with the arm structure model derived from the distribution of HMSFRs (Reid et al. 2014). We will focus on the younger population, i.e., the subsample with $2.7 < \log P < 3.0$ and $|Z| < 300$ pc, as shown in Figure 11.

The distribution shows that longer period Mira variables are located near the Sagittarius arm (red line) and the Scutum arm (blue line). Figure 11 shows that our sample concentrates to $40° < l < 60°$. This direction corresponds to the tangential direction of the Sagittarius arm and therefore the sources tend to be on the arm regardless of their distance. To investigate this effect, we examined the distance distribution of our sample in this direction. Figure 12 presents a histogram of the distances of sources located in $40° < l < 60°$ in Figure 11. There are 27 sources with $2.7 < \log P < 3.0$ in $40 < l < 60$ and $|Z| < 300$ pc, in which 23 sources (85%) are distributed in the range of 3 kpc and 8 kpc, corresponding to the Sagittarius arm. It is suggested to extend through $2 < D < 8$ kpc in the $40° < l < 60°$ (Reid et al. 2014). Another two stars are located in the range of $9 < D < 12$ kpc, corresponding to

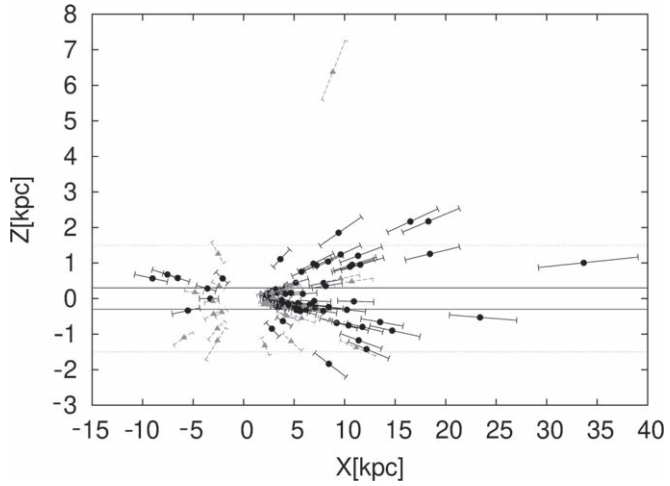

Figure 13. Edge-on distribution of our sample. Black points (circle) represent the sources with $\log P > 2.7$. Gray points (triangle) represent the sources with $\log P < 2.7$. The Galactic center is at (8, 0) and the Sun is at (0, 0). Black solid line: $|Z| = 0.3$ kpc. Black dotted line: $|Z| = 1.5$ kpc.

the Perseus arm (Reid et al. 2014). The more distant sample is likely to be incomplete because of the *IRAS* sensitivity limit.

The present result suggests that the distribution of longer period Mira variables probably trace the spiral arm structures of the Milky Way. In order to confirm our suggestion to the entire galaxy, it is necessary to search for more longer period Mira variables in other arms, for example, the Perseus arm and Outer arm.

6.2. Edge-on Distribution

The edge-on distribution of our sample is shown in Figure 13. Approximately 50% of our sample is found to exist within the Galactic plane or $|Z| < 0.3$ kpc, corresponding to the Galactic thin disk where metallicity is high, and star formation is active. We can see that the longer period Mira variables belonging to IIIa and IIIb regions in the *IRAS* two-color diagram are packed in the thin Galactic disk. Almost all the remaining 50% of sources are contained within the thick disk ($|Z| < 1.5$ kpc).

One source (IRAS 15106-1532) with a relatively shorter period (268 days) is found at 6.35 kpc from the Galactic plane. There are three possibilities of its high $|Z|$ position; (1) it was born at the Galactic plane and ejected outward, (2) born in the stream of local dwarf spheroidal galaxies (dsph) (Huxor & Grebel 2015), and (3) born in the halo of the Milky Way. In the case of (1), the stars born in the Galactic plane are randomized according to the rotation of the Milky Way over a long period of time. AGB stars like short-period Mira variables are widely distributed to the thick disk. However, it is difficult to explain IRAS 15106-1532 as having an origin in the galactic plane although it might just be an unexpected run-away star. It is necessary to create an accurate model of this moment; however, this will require taking into account the motion of stars or sudden phenomena such as blow-off from heavy stars in the Milky Way, so it is not possible to do this at the present moment. In the case of (2) stream or dsph, stars born in the dsph galaxies are pulled off by tidal force and a stream is formed. Some Mira variables are found both in the stream and in dsph galaxies (Mauron 2008; Sakamoto et al. 2012). However, the position of IRAS 15106-1532 does not match the distribution of the already known stream; therefore, IRAS 15106-1532 does not have a stream or dsph origin. In the case of (3), Whitelock (1990) reported that some Mira variables are born in a globular cluster in the halo, which are known to have short periods. It is possible to infer the origin of IRAS 15106-1532 in globular clusters in the halo.

We wish to thank the anonymous referee for a careful reading and useful comments on our manuscript. The Kagoshima University 1 m telescope is a member of the Optical and Near-infrared Astronomy Inter-University Cooperation Program and supported by it. This publication makes use of data products from the Two Micron All Sky Survey, which is a joint project of the University of Massachusetts and the Infrared Processing and Analysis Center/California Institute of Technology, funded by the National Aeronautics and Space Administration and the National Science Foundation. This publication makes use of data products from the *Wide-field Infrared Survey Explorer*, which is a joint project of the University of California, Los Angeles, and the Jet Propulsion Laboratory/California Institute of Technology, funded by the National Aeronautics and Space Administration. R.B. acknowledges support through the EACOA Fellowship from the East Asian Core Observatories Association.

ORCID iDs

Riku Urago https://orcid.org/0000-0002-6356-4255
Ross A. Burns https://orcid.org/0000-0003-3302-1935

References

Burns, R. A., Nagayama, T., Handa, T., et al. 2014, ApJ, 797, 39
Catchpole, R. M., Whitelock, P. A., Feast, M. W., et al. 2016, MNRAS, 455, 2216
Chibueze, J. O., Miyahara, T., Omodaka, T., et al. 2016, ApJ, 817, 115
Cutri, R. M., et al. 2014, yCat, 2328, 0
Dambis, A. K., Berdnikov, L. N., Efremov, Y. N., et al. 2015, AstL, 41, 489
Elias, J. H., Frogel, J. A., Matthews, K., & Neugebauer, G. 1982, AJ, 87, 1029
Feast, M. W. 2008, in First Middle East-Africa Regional IAU Meeting, ed. W. Alsabti, A. A. Hady, & V. Bothmer (Cairo: Univ. Cairo Press), 3
Feast, M. W., Glass, I. S., Whitelock, P. A., & Catchpole, R. M. 1989, MNRAS, 241, 375
Feast, M. W., & Whitelock, P. A. 2000, MNRAS, 317, 460
Glass, I. S., & Evans, T. L. 1981, Natur, 291, 303
Glass, I. S., Whitelock, P. A., Catchpole, R. M., & Feast, M. W. 1995, MNRAS, 273, 383
Gozha, M. L., & Marsakov, V. A. 2013, AstL, 39, 171
Green, G. M., Schlafly, E. F., Finkbeiner, D., et al. 2018, MNRAS, 478, 651
Green, G. M., Schlafly, E. F., Finkbeiner, D. P., et al. 2015, ApJ, 810, 25
Habing, H. J., & Olofsson, H. (ed.) 2003, Asymptotic Giant Branch Stars (Berlin: Springer)
Huxor, A. P., & Grebel, E. K. 2015, MNRAS, 453, 2653
Ita, Y., & Matsunaga, N. 2011, MNRAS, 412, 2345
Kerr, F. J. 1961, AJ, 66, 47
Lopez-Corredoira, M., Garzon, F., Hammersley, P., Mahoney, T., & Calbet, X. 1997, MNRAS, 292, L15
Matsunaga, N., Fukushi, H., & Nakada, Y. 2005, MNRAS, 364, 117
Matsunaga, N., Kawadu, T., Nishiyama, S., et al. 2009, MNRAS, 399, 1709
Mauron, N. 2008, A&A, 482, 151
Mowlavi, N., Lecoeur-Taïbi, I., Lebzelter, T., et al. 2018, A&A, 618, A58
Neugebauer, G., Habing, H. J., van Duinen, R., et al. 1984, ApJL, 278, L1
Reid, M. J., Menten, K. M., Brunthaler, A., et al. 2014, ApJ, 783, 130
Riebel, D., Meixner, M., Fraser, O., et al. 2010, ApJ, 723, 1195
Sakamoto, T., Matsunaga, N., Hasegawa, T., & Nakada, Y. 2012, ApJL, 761, L10
Schlafly, E. F., & Finkbeiner, D. P. 2011, ApJ, 737, 103
Skrutskie, M. F., Cutri, R. M., Stiening, R., et al. 2006, AJ, 131, 1163
Soszyński, I., Udalski, A., Szymański, M. K., et al. 2009, AcA, 59, 239

van der Veen, W. E. C. J., & Habing, H. J. 1988, A&A, 194, 125
Watson, C., Henden, A. A., & Price, A. 2006, SASS, 25, 47
Weiland, J. L., Arendt, R. G., Berriman, G. B., et al. 1994, ApJL, 425, L81
Whitelock, P., Feast, M., & Catchpole, R. 1991, MNRAS, 248, 276
Whitelock, P., Marang, F., & Feast, M. 2000, MNRAS, 319, 728
Whitelock, P. A. 1990, in ASP Conf. Ser. 11, Confrontation Between Stellar Pulsation and Evolution, ed. C. Cacciari & G. Clementini (San Francisco, CA: ASP), 365
Wood, P. R. 2000, PASA, 17, 18
Wright, E. L., Eisenhardt, P. R. M., Mainzer, A. K., et al. 2010, AJ, 140, 1868